LAWRENCE
LIVERMORE
NATIONAL
LABORATORY

LLNL-JRNL-401016

Computational Modeling of Blood Flow in the TrapEase Inferior Vena Cava Filter

M. A. Singer, W. D. Henshaw, S. L. Wang

February 5, 2008

Journal of Vascular and Interventional Radiology

Disclaimer

Computational Modeling of Blood Flow in theTrapEase Inferior Vena Cava Filter

Michael A. Singer, PhD, William D. Henshaw, PhD, and Stephen L. Wang, MD

From the Center of Applied Scientific Computing (MAS and WDH), Lawrence Livermore National Laboratory, Livermore, CA and The Division of Vascular and Interventional Radiology (SLW), Kaiser Permanente Santa Clara Medical Center, Santa Clara, CA

Address correspondence to: SLW; email: stephen.wang@alumni.duke.edu

Abstract

PURPOSE:
To evaluate the flow hemodynamics of the TrapEase vena cava filter using three dimensional computational fluid dynamics, including simulated thrombi of multiple shapes, sizes, and trapping positions. The study was performed to identify potential areas of recirculation and stagnation and areas in which trapped thrombi may influence intra-filter thrombosis.

MATERIALS AND METHODS:
Computer models of the TrapEase filter, thrombi (volumes ranging from 0.25mL to 2mL, 3 different shapes), and a 23mm diameter cava were constructed. The hemodynamics of steady-state flow at Reynolds number 600 was examined for the unoccluded and partially occluded filter. Axial velocity contours and wall shear stresses were computed.

RESULTS:
Flow in the unoccluded TrapEase filter experienced minimal disruption, except near the superior and inferior tips where low velocity flow was observed. For spherical thrombi in the superior trapping position, stagnant and recirculating flow was observed downstream of the thrombus; the volume of stagnant flow and the peak wall shear stress increased monotonically with thrombus volume. For inferiorly trapped spherical thrombi, marked disruption to the flow was observed along the cava wall ipsilateral to the thrombus and in the interior of the filter. Spherically shaped thrombus produced a lower peak wall shear stress than conically shaped thrombus and a larger peak stress than ellipsoidal thrombus.

CONCLUSIONS:
We have designed and constructed a computer model of the flow hemodynamics of the TrapEase IVC filter with varying shapes, sizes, and positions of thrombi. The computer model offers several advantages over in vitro techniques including: improved resolution, ease of evaluating different thrombus sizes and shapes, and easy adaptation for new filter designs and flow parameters. Results from the model also support a previously reported finding from photochromic experiments that suggest the inferior trapping position of the TrapEase IVC filter leads to an intra-filter region of recirculating/stagnant flow with very low shear stress that may be thrombogenic.

INTRODUCTION

Inferior vena cava (IVC) filters have played a critical role in the prevention of pulmonary embolism from deep venous thrombi (DVT) for over 30 years. In the United States alone, it is estimated that over 40,000 filters are placed each year (1). Over the last several years, multiple generations of filters have flooded the market, offering retrievability, lower profile delivery systems, and ease of deployment. Despite these changes and advances, successful clinical IVC filtration still hinges on a filter design that traps emboli without being inherently thrombogenic.

Decousus et al. noted an increase in recurrent DVT two years after placement of a permanent IVC filter, and suggested that this observation may be related to thrombosis at the filter site (2). To investigate this theory, a causal relationship should be established; moreover, the key relationships beg two questions: 1. Are IVC filters inherently thrombogenic?; and 2. Do IVC filters induce a prothrombotic state after trapping emboli?

The TrapEase IVC filter (Cordis, Miami Lakes, FL) is a low profile, symmetric, 6F permanent nitinol filter. Several clinical papers have evaluated the safety and efficacy of the TrapEase filter, with over 1000 patients evaluated in these reports (3-6). At least one of the studies has raised concern over possible increase in IVC thrombosis with this filter design (6). The TrapEase design incorporates a "dual filtration" system with two trapping positions: one inferiorly, which traps emboli along the wall of the IVC; and one superiorly, which traps emboli in the central cone. Recent papers have evaluated the hemodynamics of the TrapEase filter in an in- vitro setting using the photochromic flow visualization technique; the findings suggest that trapping emboli in the inferior trapping position may lead to a prothrombotic state (7-8).

In this study, we have designed and constructed computer models of the flow hemodynamics of the TrapEase IVC filter both free of thrombus and with various thrombus volumes, shapes, and trapping positions. Using these models, we have computed the wall shear stress and velocity contours under various conditions and identified regions of flow stagnation and recirculation. This information may be valuable in predicting clinical success and failure.

MATERIALS AND METHODS

Computer models of the IVC, TrapEase filter, and simulated thrombi were constructed to study the flow dynamics. Flow around the unoccluded and partially occluded filter was simulated using three-dimensional computational fluid dynamics. All computations were performed on one processor of a supercomputer with 640 Opteron (AMD, Sunnyvale, CA) processors (multiple single-processor simulations were run simultaneously); the machine resides at the Lawrence Livermore National Laboratory (Livermore, CA).

IVC MODEL

The IVC was modeled as a straight pipe. The diameter of the pipe was 23 mm, per the average IVC diameter described by Kaufman et al. (9). The length of the pipe was 90 mm; this length provided adequate distance for the parabolic inlet velocity profile to develop fully before reaching the filter. The sides of the pipe were no-slip boundaries (i.e., zero velocity), and the outflow boundary condition used a mixed (Robin) condition on the pressure and an extrapolation of the velocity.

FILTER MODEL

Computer aided design (CAD) was used to construct a geometrically accurate model of the TrapEase filter. First, the filter was inserted into a 23 mm inner diameter glass test tube, which compressed the filter as though it were in an IVC of the same diameter. Then, high resolution photographs were taken of the filter using a Dimage Xt (Minolta, Osaka, Japan) digital camera. Measurements of the filter were also obtained with a Cen-Tech 6-inch digital caliper (Harbor Freight Tools, Camarillo, CA). The photographs and measurement data were then imported into the GNU Image Manipulation Program (GIMP) (www.gimp.org) where spatial geometry of the filter was extracted based on pixel color and location. The geometric specifications were then imported into the Overture software framework (Lawrence Livermore National Laboratory, Livermore, CA) (10,11) where a CAD model was constructed. For ease in modeling, the barbs on the filter were excluded from the model since their presence does not alter the characteristics of the flow, as they are extralumenal.

SIMULATIONS

The flow was modeled as an incompressible, Newtonian fluid whose motion is described mathematically by the Navier-Stokes (NS) equations (12). The NS equations were solved using the incompressible flow solver within the Overture software framework (available for download at http://computation.llnl.gov/casc/Overture). Overture uses the method of overset grids to discretize the equations using a collection of curvilinear meshes and then solves the equations using finite difference approximations (13). For the present work, second-order accurate spatial approximations were used, and the spatial resolution of the solution was 2 mm or less. The steady-state solution was obtained using a pressure-based equation solver (14,15). Post processing was performed using tools provided by Overture; custom scripts written in Matlab (MathWorks, Natick, MA) and the GIMP were also used.

Simulations of the partially occluded filter were conducted with 0.25mL, 0.50mL, 1mL, 1.5mL, 1.875mL, and 2.0mL spherical thrombi in the superior trapping position, and 0.25mL and 0.50mL spherical thrombi in the inferior trapping position. Conical and ellipsoidal clots of 1.875mL were also placed in the superior trapping position. The thrombi were incorporated into the simulations by using Overture's CAD capabilities.

For the problem being considered, the single non-dimensional parameter that describes the flow configuration is the Reynolds number, $Re = \rho U D / \mu$. Here, $\rho = 1040$ kg/m^3 is the density of blood, U is the mean inlet velocity, D = 23 cm is the diameter of the vena cava, and $\mu = 2.57e\text{-}3$ kg/(ms) is the viscosity of blood. All of the results presented here used U = 6.45 cm/s so that Re = 600; Re = 600 has been utilized in multiple previously published reports involving vena cava experiments (7,16,17). Setting Re = 600 corresponds to a blood flow rate of 2 L/min in a 2 cm vena cava (7).

RESULTS

The three-dimensional Navier-Stokes equations were solved for the velocity (three components) and the pressure. Contour plots of the axial component of velocity were normalized by the theoretical average velocity, in the axial direction, for fully-developed flow in a long straight pipe (i.e., Poiseuille flow). In the discussion to follow, all references to flow velocity refer to the axial component of the velocity. The wall shear stress was computed as the product of the viscosity and the transverse gradient of the axial velocity; velocity gradients in the tangential directions were negligible. All wall shear stresses were similarly normalized by the theoretical value for pipe flow. In all figures, flow is left-to-right.

UNOCCLUDED FILTER

The velocity contours and wall shear stress for the unoccluded filter are shown in Figure 1a; the velocity is shown on two planes that slice the geometric center of the filter and vein. Figure 1b illustrates the flow near the inferior (top image) and superior (bottom image) tips. Figure 1 demonstrates excellent symmetry of the flow in and around the filter. This result was expected since the filter was placed in the geometric center of the IVC model, and the filter was free of tilt; cross sectional slices of the velocity contours (not shown) further demonstrated flow symmetry. In Figure 1a, the peak normalized velocity of 2.05 occurred upstream of the filter; flow inside the filter had a normalized velocity in the range 0.95-1.85. Further, the velocity at the cava wall and the surface of the filter was zero, as expected for viscous flow. Disruption of the flow, due to the filter, was minimal, except immediately downstream of both filter tips. Note that the filter tips have a hallow core, which allows some flow to pass through. Flow disruption downstream of the superior tip was more pronounced than the upstream tip. As seen in Figure 1b, a large region of nearly stagnant flow, with a normalized velocity less than 0.25, was observed downstream of the superior tip; areas of negative velocity, indicating recirculation, were also observed.

From the wall shear stress shown in Figure 1a, a normalized peak value of 2.15 was observed near the superior “hips” of the filter. Near the inferior “hips,” a peak stress of 2.1 was observed. Both stresses are within 15% of those reported by Leask et al. (7). Between the inferior and superior "hips," the wall shear stress relaxes towards that of Poiseuille flow as the flow inside the filter increased momentum thereby decreasing the velocity gradient near the wall to maintain conservation of mass.

PARTIALLY OCCLUDED FILTER: A. SUPERIOR THROMBI

Velocity contours and wall shear stresses for the partially occluded filter with 0.25mL, 0.50mL, 1mL, 1.875mL, and 2mL spherical thrombi in the superior position are shown in Figures 2-6. The figures demonstrate that larger thrombi induced a monotonically increasing peak flow velocity: increasing the volume by a factor of 8 increased the peak velocity by 20%. In all cases, the peak velocity occurred at the location of minimum distance between the thrombus and the wall of the cava. The rise in peak velocity was due to the reduction in cross sectional area through which the flow could pass. Larger thrombus also produced larger regions of low velocity flow downstream of the thrombus, and all thrombi disrupted the flow inside the filter. In all cases, regions of recirculating flow downstream of the superior tip (demonstrated by regions of negative velocity) were observed, and the axial and transverse lengths of the recirculation zones increased with thrombus volume. For all thrombus volumes considered, the largest negative velocities occurred downstream of the superior tip.

The peak wall shear stress increased monotonically with thrombus volume and always occurred downstream of the peak velocity. This was because flow around the clot forced fluid toward the wall of the cava thereby producing a steep velocity gradient due to mass conservation. A rise in wall shear stress was also observed near the upstream "hips" of the filter, but the peak value was nearly independent of thrombus volume. Figure 6 compares profiles of wall shear stresses for all thrombus volumes (including those for which velocity contours are not shown); the peak stress moved upstream in proportion to the increase in thrombus volume.

PARTIALLY OCCLUDED FILTER: B. INFERIOR THROMBI

Figures 8 and 9 show velocity contours and wall shear stresses for 0.25mL and 0.50mL spherical thrombi placed in the inferior trapping position. As demonstrated, the peak velocity increased by 5% with a 100% increase in thrombus volume. In both cases, flow in the upper half of the filter remained virtually undisturbed, while flow in the lower half was disrupted throughout the axial length of the filter. Flow behind each thrombus showed low velocity and a region of slow moving flow extended to the superior “hips” in both cases. Axial flow near the centerline showed greater disruption for the 0.50mL case due to the larger radius of the thrombus. Regions of recirculating flow were observed near the cava wall ipsilateral to the thrombus. Velocity contours near the superior tip were similar to those of the unoccluded filter indicating that the flow downstream of the filter behaved as though no thrombus was present.

The shear stresses along the walls opposite and ipsilateral to each thrombus are also shown in Figures 8-9. For the wall opposite the thrombi, the peak normalized stresses were within 10% for both sizes of thrombus, and the location of peak stress was downstream of each thrombus near the inferior “hips.” The similarity in peak stress and location was consistent with the similarity in velocity contours in the top half of each

filter. A second peak in wall shear stress of 2.1 was observed near the superior “hips” of the filter for both thrombi. The corresponding peak for the unoccluded filter was 2.15, further demonstrating the minimal disruption to the flow in the upper half of the filter.

The shear stresses on the walls ipsilateral to each thrombus were lower than the corresponding stresses on the opposite wall, except in close proximity to the thrombi. Inferior to each thrombus, the shear stress decreased to zero as the thickness of the boundary layer increased, thereby decreasing the velocity gradient along the wall. Upstream of the thrombus, a region of flow reversal was observed that resulted in a point of zero wall shear stress inferior to the thrombus. The shear stress immediately inferior and superior to the thrombus exhibited a complex oscillatory pattern due to the thrombus forcing flow away from the ipsilateral cava wall. As a result, the thickness of the boundary layer varied, recirculating flow was observed, and the flow became highly three-dimensional; the reported values of shear stress provided a qualitative picture of the complex flow. Downstream of the thrombus, the normalized wall shear stress remained below unity for the 0.25mL thrombus and below 0.75 for the 0.50mL thrombus until the superior “hips” was encountered farther downstream. In both cases, the disturbance caused by the thrombi diminished downstream of the superior “hips,” and the flow regained momentum along the ipsilateral wall. A corresponding rise in wall shear stress was observed, although the stress remained lower than that observed on the opposite wall.

PARTIALLY OCCLUDED FILTER: C. CONICAL AND ELLIPSOIDAL THROMBI

Figure 10 and 11 illustrate velocity contours and wall shear stresses for 1.875mL conical and ellipsoidal thrombi in the superior trapping position, respectively. As demonstrated, a peak velocity of 2.5 was observed for the conical thrombus, and the ellipsoidal thrombus had a peak velocity of 2.12; the spherical thrombus of the same volume (Figure 5) demonstrated a maximum velocity of 2.47. The conical thrombus produced a region of stagnant and recirculating flow near the superior tip of the filter that contained a larger volume of fluid than the ellipsoidal thrombus, but a smaller volume than the spherical thrombus. The ellipsoidal thrombus, due to its streamlined shape, disrupted the flow the least of the three shapes as exhibited by relatively small (both axial and transverse) and well-confined regions of disturbance both upstream and downstream of the thrombus. It should be noted, however, that thrombi are not likely to be trapped in an ellipsoidal shape due to a lack of side supports from the TrapEase filter. Nonetheless, our modeling infrastructure facilitated the examination of different clot shapes for comparison.

The wall shear stresses for all three shapes were qualitatively similar and are compared in Figure 12. The upstream peak near the inferior "hips" of the filter had a normalized value of 2.5 for the conical and elliptical thrombi and 2.2 for the spherical thrombus. The downstream peak stress for the ellipsoidal thrombus was 4.8 while the spherical and conical thrombi produced peak stresses near 7.5 and 8.5, respectively. The location of the peak stresses was similar for all three thrombi with the ellipsoidal

thrombus having a peak approximately 3mm farther downstream due to the downstream jump in velocity gradient near the point where the thrombus and filter meet.

DISCUSSION

In 1856, Virchow described a triad of factors leading to venous thrombosis: 'abnormalities of the blood vessel wall', 'abnormalities of the blood constituents,' and 'abnormalities of blood flow.' A modern interpretation of these three components corresponds to abnormalities of the endothelium, abnormalities of platelets and the coagulation/fibrinolytic pathways, and abnormalities in blood flow or vessel stenosis (18). The biochemical signaling pathways that mediate venous and arterial thrombosis are multifactorial and complex. Over the last 30 years, Virchow's triad has gathered more proof as the complex relationships between shear stress and platelet-dependent hemostasis have become elucidated (19). With over 40,000 IVC filters placed annually in the United States, understanding the hemodynamics of IVC filters is critical to identifying any potential thrombogenic risk. In this study, we have designed and constructed a computer model of the flow hemodynamics of the TrapEase IVC filter with varying shapes, sizes, and placements of model thrombi. Our simulations provide valuable information on potential risk factors, and our results illustrate the ability of computer models to provide insight into flow characteristics of clinical importance.

Our results demonstrate that in the unoccluded TrapEase IVC filter, there is symmetry of flow in and around the filter with a region of recirculating/stagnant flow immediately downstream of the superior tip of the filter (Figure 1). The TrapEase filter has two trapping positions, an inferior trapping position that traps thrombus along the side of the filter against the cava wall, and a superior trapping position that traps thrombus centrally, within the superior cone of the filter. In the partially occluded filter, the velocity of flow immediately downstream of thrombi in both trapping positions was reduced and areas of recirculation were observed. However, in the partially occluded filter with 0.25mL spherical thrombus, the shear stress along the wall opposite the thrombus was significantly higher around thrombus in the superior trapping position (3.25 normalized shear stress) (Figure 2) compared to the inferior trapping position (2.3 normalized shear stress) (Figure 8); along the cava wall ipsilateral to the thrombus, normalized shear stress dropped significantly to as low as 0.25 near the thrombus. Low flow velocities and areas of recirculation were seen in the partially occluded filter extending approximately 2 cm downstream from each trapping position. In the superior trapping position, the low flow velocity is located in the central portion of the cava (Figures 2-6); however, in the inferior trapping position, the low flow velocity is located in the periphery within the filter, along the cava wall (Figures 8-9). Increases in thrombus volume produced an exponential increase in normalized shear stress (Figure 7). Differences in thrombus shapes showed the conical shape caused a larger region of stagnant/recirculating flow, and the ellipsoid shape disrupted flow the least.

The differences in shear stress and locations of low velocity/recirculating flow between the two trapping positions may be clinically important. Platelets are preferentially concentrated near the vessel wall, away from the central flow (20). High

shear stresses can activate platelets (though typically at arterial shear stress levels) (19) resulting in platelet adhesion and primary hemostasis, but this can be balanced by high shear stresses which enhance the removal of thrombin and fibrin thereby reducing the likelihood of secondary hemostasis (20). High levels of shear stress have also been associated with stimulation of endothelial cells that secrete tissue plasminogen activator (tPA) and reduce the risk of hemostasis (19). Areas of recirculating blood flow under low shear stresses can lead to venous thomboembolism (20). In our model, with thrombus in the inferior trapping position, there is a region of low flow velocity along with recirculation within the filter, along the cava wall adjacent to the thrombus. The low shear stress along the cava wall in this inferior trapping position may allow enough stagnation that thrombin and fibrin could accumulate, and secondary hemostasis may be initiated. Conversely, with high shear stress surrounding the thrombus in the superior, central trapping position, secondary hemostasis would be more difficult to initiate as thrombin and fibrin are cleared and mechanical lysis can occur.

Leask et al. performed an in vitro, bench evaluation of the hemodynamic effects of clot entrapment of the TrapEase IVC filter using a photochromic technique (7). Our velocity contour maps and shear stress calculations for the unoccluded filter are similar, thereby corroborating our methods. Our computer model offers several advantages over the photochromic technique and in vitro testing in general: the spatial resolution of our results is 0.2 mm and we can increase the resolution if desired, while the results in Leask et al. are 0.5 mm; the computer model allows one to evaluate different sizes, shapes, locations, and configurations of thrombi without having to rerun expensive and time consuming bench experiments; flow characteristics such as inflow velocity and viscosity of blood are easily modified; quantities that are difficult to evaluate experimentally (e.g., pressure, transverse velocities) are accurately computed; and our computer model establishes a platform that is readily adaptable to evaluate new filter designs without physically constructing the filter and performing the time/labor intensive bench experiments. As an example of the benefits provided by our modeling framework, we note a region of recirculation downstream of the superior tip of the unoccluded TrapEase IVC filter. This was not previously described by Leask et al. and may be a result of the improved resolution of our computer model.

Our computer model is founded on simplifying yet realistic assumptions. The model assumes that flow through the IVC is steady. Compared to the aorta, the flow in the IVC experiences lower pulsatility due to a damping of the pulse pressure by the time blood reaches the venous system (21). Flow in the IVC is also unidirectional (21). The wall of the cava is modeled as smooth and rigid, and inflow from renal, lumbar, and other venous tributaries is excluded; in vivo results (e.g., from CT scans) suggest that the vena cava is dynamic and maintains a complex topology that is specific to each patient. The simulated thrombi are solid and are constructed from spheres, ellipses, and cones; in vivo clots assume random shapes with variable elasticity and porosity. As noted in Swaminathan et al (22), however, spherical thrombi represent, in some sense, a statistical average of irregular shapes. Finally, our model assumes that the flow is laminar and blood is Newtonian: viscosity is a function of the local shear rate. Although blood is generally thought to be non-Newtonian, Swaminathan et al. found that non-Newtonian

effects for flow in the IVC are minimal (22). Our modeling infrastructure is capable of addressing the issues described above by incorporating additional realism based on in vitro or in vivo data (e.g., flow velocities, CT scans).

A preliminary clinical study of the TrapEase IVC filter raised questions of an increased risk of caval thrombosis (23). In this study, 189 patients were evaluated and three were noted to have IVC thrombosis (1.5%) (23). A current review of the literature shows four clinical studies of the TrapEase IVC filter with a total of 1,047 patients (23-26). Taken as a whole, eight patients (0.76%) demonstrated total or near total IVC occlusion. Amongst all IVC filters, reported ranges of filter related IVC occlusion vary widely from 0-28% (27); moreover, 0.76% is considerably less than the average reported rates of caval occlusion for many other IVC filters (28). Therefore, based on current clinical data, the concern for increased rates of total caval thrombosis with the TrapEase IVC filter is unfounded.

The largest clinical study of the TrapEase filter reported a total of 751 patients, of whom 270 patients had follow-up abdominal CTs (24). Within this group of 270, 68 patients (25.2%) had non-occlusive thrombus noted within the filter. Though this percentage is seemingly high, other TrapEase published clinical papers did not report follow-up on intra-filter, non-occlusive thrombus (23,25,26) However, two recent publications regarding the retrievable version of the TrapEase filter, the Optease (Cordis, Miami Lakes, FL), have reported rates of non-occlusive thrombus in the 26-39% range (29,30). The Optease filter and TrapEase filter are essentially structurally identical except for unidirectional barbs and a hook at the inferior end of the Optease. In contrast, two recent reports on the Gunther Tulip retrievable filter (Cook, Bloomington, IN) show non-occlusive intra-filter thrombus rates of 12-19% (31,32) . Reporting standards of non-occlusive thrombus are not uniform and therefore these numbers are difficult to compare; but a single-center comparison with the Gunther Tulip has been published (29). In this study, 92 patients were treated with Gunther Tulip filter and 80 patients were treated with the Optease filter. Rates of nonocclusive intrafilter thrombus were 21% for the Gunther Tulip and 39% for the Optease. In particular, smaller thrombi (<25% of the IVC diameter) were seen in 31% of Optease filters and only 8% of Gunther tulip filters ($p=0.002$) (29). These studies support our experimental findings as well as those of Leask et al., that the inferior trapping position against the cava wall results in stagnation and recirculation and may promote intra-filter thrombosis (7). Further research into the short-term and long-term clinical effects of non-occlusive intra-filter thrombus should be pursued.

CONCLUSION

We have designed and constructed a computer model of the flow hemodynamics of the TrapEase IVC filter with varying shapes, sizes, and positions of thrombi. Our methods are corroborated by previously published photochromic results by Leask et al. The computer model offers several advantages over in vitro techniques including: improved resolution, ease of evaluating different thrombus sizes and shapes, and easy adaptation for new filter designs and flow parameters. Results from the model also

support a previously reported finding from photochromic experiments that suggest the inferior trapping position of the TrapEase IVC filter leads to an intra-filter region of recirculating/stagnant flow with low shear stress that may be thrombogenic. Evaluation of the current clinical literature does not show increased rates of total IVC thrombosis in patients with the TrapEase IVC filter relative to other filter types; however, there is a higher rate of intra-filter, non-occlusive thrombus in several studies of the nearly structurally identical Optease retrievable filter, which deserves further evaluation.

ACKNOWLEDGEMENTS

This work was performed under the auspices of the U.S. Department of Energy (DOE) by Lawrence Livermore National Laboratory (LLNL) in part under Contract W-7405-Eng-48 and in part under Contract DE-AC52-07NA27344 and by DOE contracts from the ASCR Applied Math Program. Computer time on LLNL's Yana cluster was provided under Livermore Computing's Multiprogrammatic & Institutional Computing Initiative. LLNL is operated by Lawrence Livermore National Security, LLC, for the DOE, National Nuclear Security Administration under Contract DE-AC52-07NA27344.

REFERENCES

1. Magnant JG, Walsh DB, Juravsky LI, Cronenwett JL. Current use of inferior vena cava filters. J. Vasc. Surg 1992; 16:701-6.

2. Decousus, H, Leizorovicz, A., Parent, F., Page, Y. et al. A clinical trial of vena cava filters in the prevention of pulmonary embolism in patients with proximal deep vein thrombosis. NEJM 1998; 338:409-415.

3. Rousseau H, Perreault P, Otal, P et al. The 6F-nitino TrapEase inferior vena cava filter: results of a prospective multicenter trial. J Vasc Intervent Radiol 2001; 12:299-304.

4. Liu WC, Do YS, Choo SW, et al. The mid-term efficacy and safety of a permanent nitinol IVC filter (TrapEase). Korean J Radiol 2005; 6:110-116.

5. Kalva SP, Wicky S, Waltman AC, et al. TrapEase vena cava filter: Experience in 751 patients. J Endovasc Ther 2006; 13:365-372.

6. Schutzer R, Ascher E, Hingorani A, et al. Preliminary results of the new 6F TrapEase inferior vena cava filter. Ann Vasc Surg 2003; 17:103-106.

7. Leask RL, Johnston KW, Ohja M. Hemodynamic effects of clot entrapment in the TrapEase inferior vena cava filter. J Vasc Intervent Radiol 2004; 15:485-490.

8. Harlal A, Ohja M, Johnston KW. Vena cava filter performance based on hemodynamics and reported thrombosis and pulmonary embolism patterns. J Vasc Intervent Radiol 2007; 18:103-115.

9. Kaufman, JA, Waltman, AC, Rivitz, SM, Geller SC. Anatomical observations on the renal veins and inferior vena cava at magnetic resonance angiography. Cardiovasc Intervent Radiol 1995; 18:153-157.

10. Brown DL, Henshaw WD, Quinlan DJ. An object oriented framework for solving partial differential equations. Scientific Computing in Object-Orientied Parallel Environments, Springer Lecture Notes in Computer Science; 1343:177-194.

11. Henshaw WD, Schwendeman DW. Moving overlapping grids with adaptive mesh refinement for high-speed reactive and non-reacting flow. J Comp Phys 2006; 216(2):744-779.

12. Batchelor GK. An introduction to fluid dynamics. Cambridge University Press, Cambridge 1980.

13. Chesshire GS, Henshaw WD. Composite overlapping meshes for the solution of partial differential equations. J Comp Phys 1990; 90(1):1-64.

14. Henshaw WD. A fourth-order accurate method for the incompressible Navier-Stokes equations on overlapping grids. J Comp Phys 1994; 113(1):13-25.

15. Henshaw WD, Petersson NA. A split-step scheme for the incompressible Navier-Stokes equations. In: Hafez MM, ed. Numerical Simulation of Incompressible Flows, World Scientific 2003; 108-125.

16. Leask RL, Johnston KW, Ojha M. In vitro hemodynamic evaluation of a simon nitinol vena cava filter: possible explanation of IVC occlusion. J Vasc Interv Radiol 2001; 12:613-618.

17. Harlal A, Ojha M, Johnston KW. Vena cava filter performance based on hemodynamics and reported thrombosis and pulmonary embolism patterns. J Vasc Interv Radiol 2007; 18:103-115.

18. Chung I and Lip G. Virchow's triad revisited: blood constituents. Pathophysiol Haemost Thromb 2003/2004; 33: 449-454.

19. Kroll MH, Hellums JD, Mcintire LV, Schafer AI, Moake, JL. Platelets and shear stress. Blood 1996; 88: 1525-1541.

20. Lowe G. Virchow's triad revisited: abnormal flow. Pathophysiol Haemost Thromb 2003/2004; 33: 455-457.

21. Cheng CP, Herfkens RJ, Taylor CA. Inferior vena cava hemodynamics quantified in vivo at rest and during cyclic exercises using magnetic resonance imaging. Am J Physiol Heart Circ Physiol 2003; 284:1161-1167.

22. Swaminathan TN, Hu HH, Patel AA. Numerical analysis of the hemodynamics and embolus capture of a Greenfield vena cava filter. J Biomed Eng 2006; 128:360-370.

23. Schutzer R, Ascher E, Hingorani A, Jacob T, Kallakuri S. Preliminary results of the new 6F Trapease inferior vena cava filter. Ann Vasc Surg 2003; 17:103-106. Rousseau H, Perreault P, Otal P, et al. The 6-F nitinol TrapEase inferior vena cava filter: results of a prospective multicenter trial. J Vasc Interv Radiol 2001; 12:299-304.

24. Kalva SP, Wicky SW, Waltman AC, Athanasoulis, CA. TrapEase vena cava filter: experience in 751 patients. J Endovasc Ther 2006; 13:365-372.

25. Liu WC, Do YS, Choo SW, et al. The mid-term efficacy and safety of a permanent nitinol IVC filter (TrapEase). Korean J Radiol 2005; 6:110-6.

26. Rousseau H, Perreault P, Otal, P, et al. The 6-F nitinol TrapEase inferior vena cava filter: results of a prospective multicenter trial. J Vasc Interv Radiol 2001; 12:299-304.

27. Streiff MB. Vena caval filters: a comprehensive review. Blood 2000; 95: 3669-3677.

28. Kinney TB. Update on inferior vena cava filters. J Vasc Interv Radiol 2003; 14: 425-440.

29. Keller IS, Meier C, Piffner R, et al. Clinical comparison of two optional vena cava filters. J Vasc Interv Radiol 2007; 18:505-511.

30. Oliva VL, Szatmari F, Giroux M, et al. The Jonas Study: Evaluation of the retrievability of the Cordis OptEase inferior vana cava filter. J Vasc Interv Radiol 2005; 16: 1439-1445.

31. Hoppe H, Nutting CW, Smouse HR, et al. Gunther Tulip filter retrievability multicenter study including CT follow-up: final report. J Vasc Interv Radiol 2006; 17: 1017-1023.

32. Wicky S, Doenz F, Meuwly J, et al. Clinical experience with retrievable Gunther Tulip vena cava filters. J Endovasc Ther 2003; 10:994-1000.

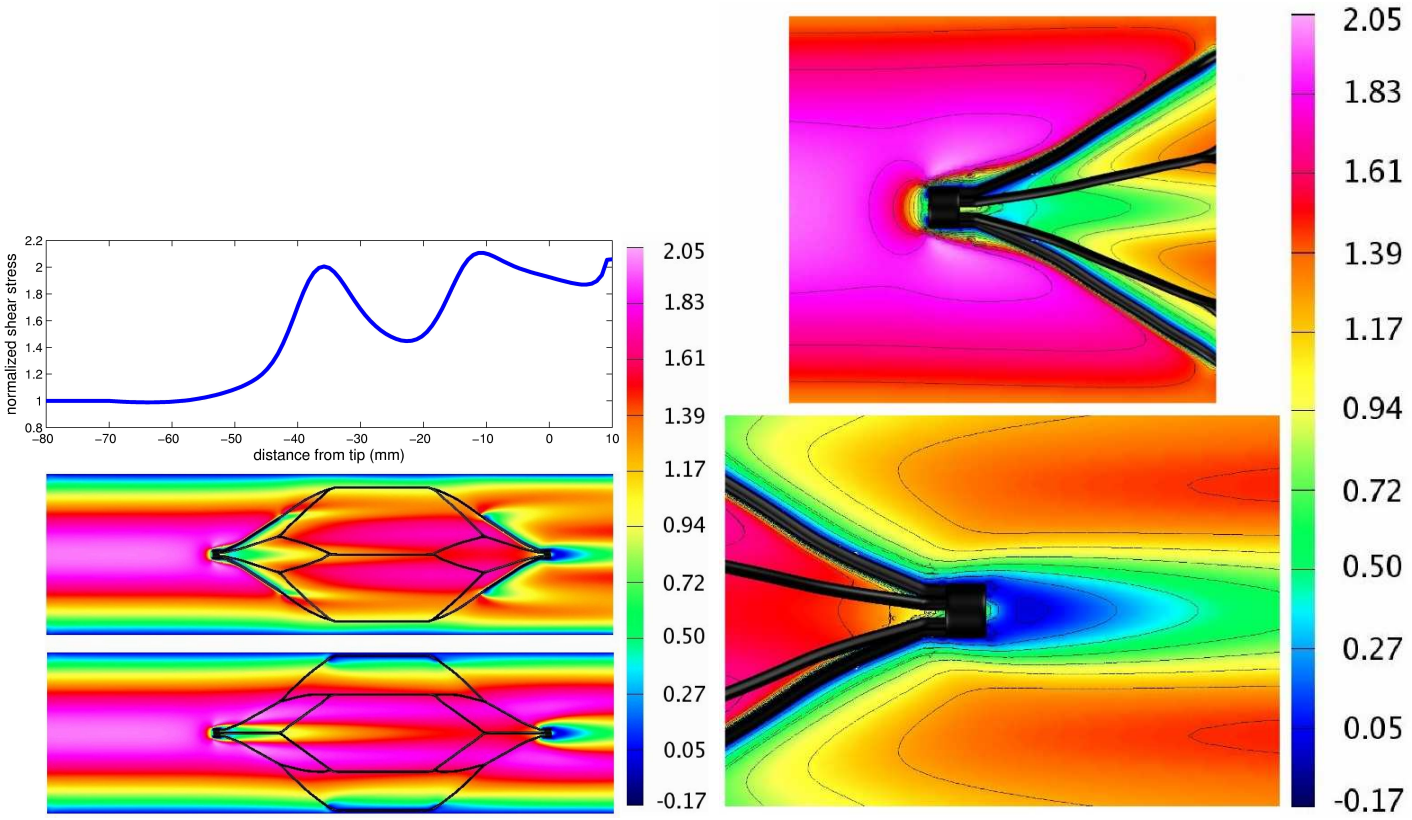

Figure 1: Pipe with TrapEase filter: (a) normalized shear stress and axial velocity contours; (b) flow near the inferior (top) and superior (bottom) tips.

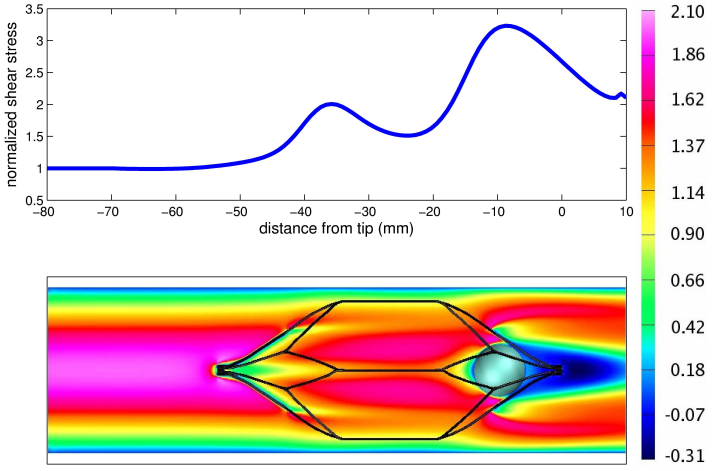

Figure 2: Pipe with TrapEase filter and 0.25mL spherical thrombus.

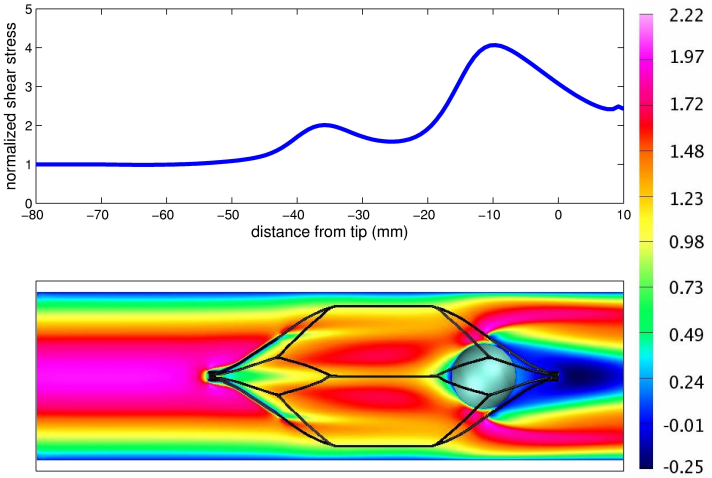

Figure 3: Pipe with TrapEase filter 0.50mL spherical thrombus.

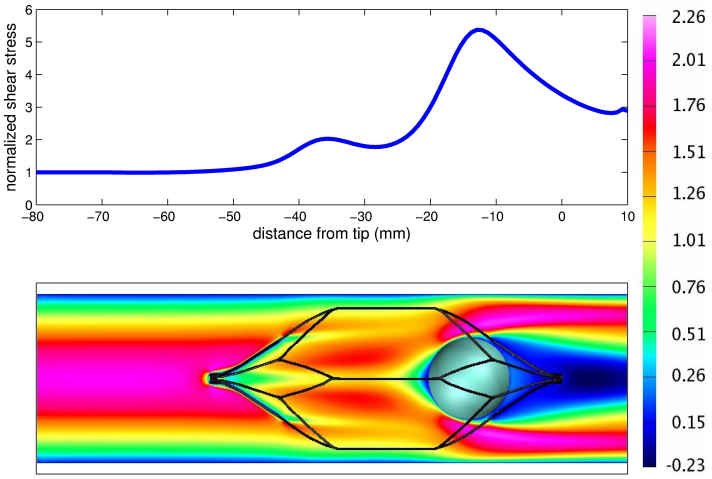

Figure 4: Pipe with TrapEase filter and 1mL spherical thrombus.

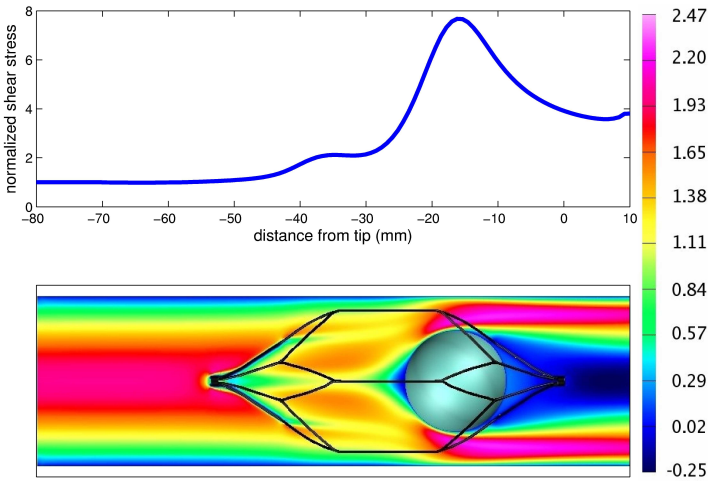

Figure 5: Pipe with TrapEase filter and 1.875mL spherical thrombus.

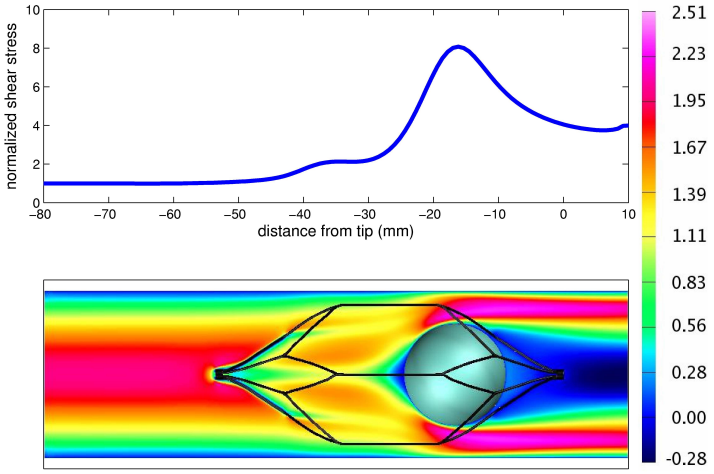

Figure 6: Pipe with TrapEase filter and 2mL thrombus.

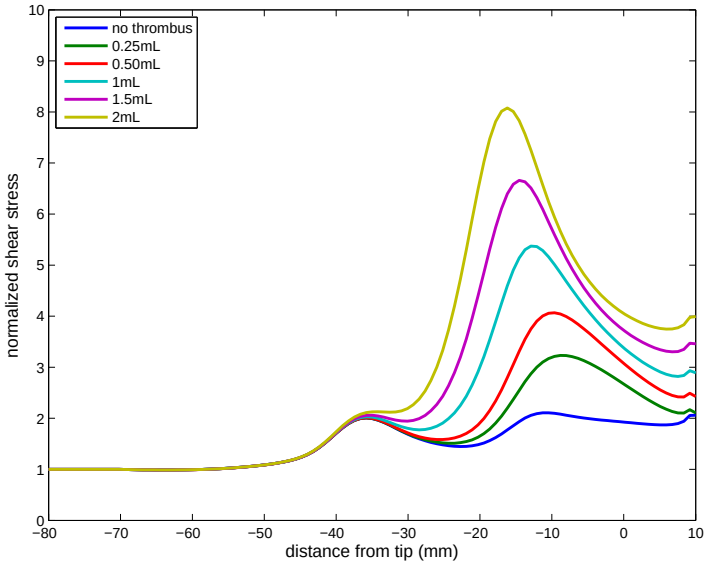

Figure 7: Comparison of wall shear stresses for different sizes of spherical thrombi.

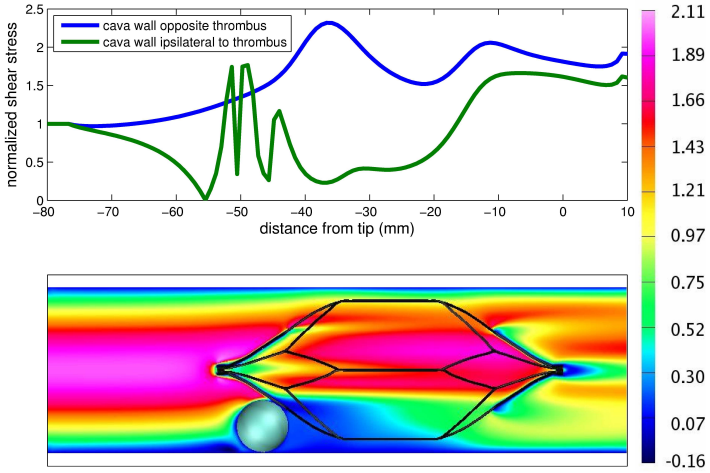

Figure 8: Pipe with TrapEase filter 0.25mL spherical thrombus.

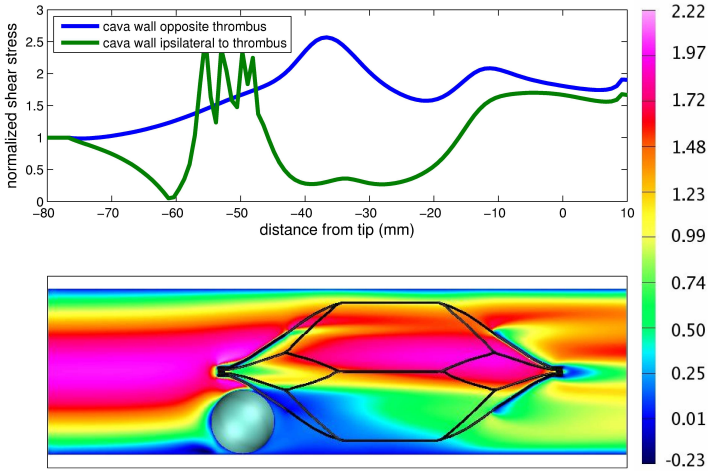

Figure 9: Pipe with TrapEase filter 0.50mL spherical thrombus.

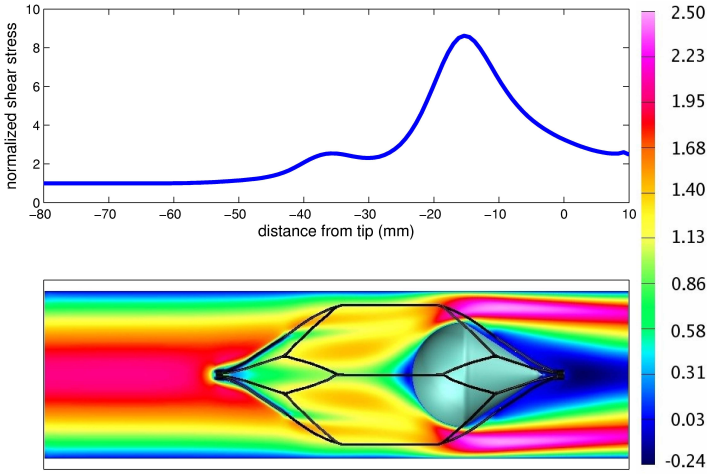

Figure 10: Pipe with TrapEase filter and 1.875mL thrombus conical thrombus.

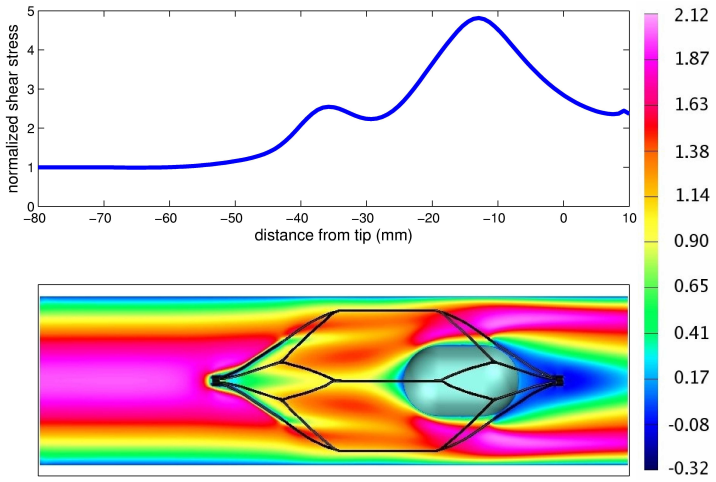

Figure 11: Pipe with TrapEase filter and 1.875mL thrombus ellipsoidal thrombus.

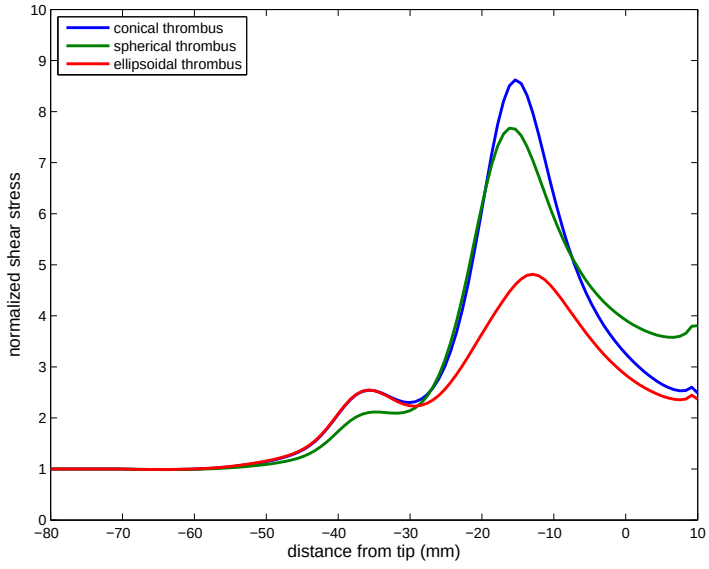

Figure 12: Comparison of wall shear stresses for different shapes of thrombi.